Process Biochemistry 48 (2013) 1724–1735

Contents lists available at ScienceDirect

Process Biochemistry

journal homepage: www.elsevier.com/locate/procbio

Preparation of sulfonated poly(ether–ether–ketone) functionalized ternary graphene/AuNPs/chitosan nanocomposite for efficient glucose biosensor

Jay Singh[a,d], Partha Khanra[a], Tapas Kuila[b], Manish Srivastava[a], Ashok K. Das[a], Nam Hoon Kim[c], Bong Joo Jung[a], Da Yeong Kim[a], Seung Hee Lee[a,d,*], Dong Won Lee[a], Dae-Ghon Kim[e], Joong Hee Lee[a,c,d,*]

[a] WCU Program, Department of BIN Fusion Technology, Chonbuk National University, Jeonju, Jeonbuk 561-756, Republic of Korea
[b] Surface Engineering & Tribology Division, CSIR—Central Mechanical Engineering Research Institute, Durgapur 713209, India
[c] Department of Hydrogen and Fuel Cell Engineering, Chonbuk National University, Jeonju, Jeonbuk 561-756, Republic of Korea
[d] BIN Fusion Research Center, Department of Polymer/Nano Science and Technology, Chonbuk National University, Duckjin-dong 1Ga 664-14, Jeonju, Jeonbuk 561-756, Republic of Korea
[e] Medical School, Chonbuk National University, Jeonju, Jeonbuk 561-756, Republic of Korea

ARTICLE INFO

Article history:
Received 7 May 2013
Received in revised form 12 July 2013
Accepted 30 July 2013
Available online 8 August 2013

Keywords:
Sulfonated graphene
Chitosan
Glucose
Electrochemical studies
Sensors

ABSTRACT

A facile method of preparing water-dispersible sulfonated graphene (SPG) using sulfonated poly(ether–ether–ketone) organic polymer as a modifier was realized. A glucose biosensor was fabricated by immobilizing glucose oxidase (GO_x) on the surface of AuNPs used to modify SPG and chitosan (CH) deposited on an indium tin-oxide (ITO) glass electrode by a solution casting method. Morphological and structural characterizations confirm that the AuNPs can be efficiently applied to the SPG–CH matrix. The amperometric response of the GO_x/SPG–AuNPs–CH/ITO bioelectrode shows a broad linear range of 0.5 to 22.2 mM, with a limit of detection of 0.13 mM and a high sensitivity of 6.51 μA/(mM cm^2). The excellent performance of the constructed biosensor is attributed to the large surface-to-volume ratio and electron transfer ability of SPG, the high catalytic activity of the AuNPs, and the good biocompatibility of CH. In addition, the sensor has important advantages, such as its simple preparation, fast response time (10 s), good stability (70 days), and high reproducibility. Favorable results upon examining the electrochemical response for the determination of glucose in human blood serum were obtained, without the assistance of a negligible effect of interfering bio-analytes. The results of studies show that the ternary SPG–AuNPs–CH nanocomposite may offer a new approach for developing novel types of highly sensitive and stable electrochemical biosensors.

1. Introduction

Graphene has attracted significant attention since its discovery in 2004, not only in the field of basic research, but also in technological applications, due to its unique features, such as its quantum Hall effect [1], excellent mechanical flexibility, thermal stability, optical transparency, and electrical properties [2]. In recent years, the rapid development of graphene-based optoelectronic devices [3], supercapacitors [4], gas sensors [5], pH sensors [6], chemical sensors [7], biosensors [8,9], and nanocomposites [10] has garnered much attention. Graphene has received enormous interest in various areas of research, owing to its large specific surface area, extraordinary electrical and thermal conductivities [11], high mechanical stiffness [12], good biocompatibility [13], and low manufacturing cost [14]. The biocompatibility, high conductivity, and large surface area of graphene make it an ideal choice for the development of highly sensitive electrochemical biosensors and bioelectronic devices [15–18]. Moreover, graphene is known to promote the electron transfer for the redox reaction of redox proteins, and redox enzymes immobilized on graphene retain their enzymatic activity [19]. Such properties indicate that graphene may be a good support for electrocatalysts.

Various nano–bio interfaces have been realized in the areas of biological device design, biomolecules detection, bioassays, and molecular medicine [20]. Graphene has been employed as a substrate for various biomolecules and cells [21]. Surface modification

* Corresponding authors. Tel.: +82 63 270 2342; fax: +82 63 270 2341.
E-mail addresses: lsh1@jbnu.ac.kr (S.H. Lee), jhl@jbnu.ac.kr (J.H. Lee).

1359-5113/$ – see front matter © 2013 Elsevier Ltd. All rights reserved.
http://dx.doi.org/10.1016/j.procbio.2013.07.025

is prerequisite to improving the biocompatibility, solubility, and selectivity of graphene. Hence, several studies have focused on the surface modification and chemical functionalization of graphene [22,23]. Recently, Schniepp et al. developed a new approach for the synthesis of functionalized graphene sheets (FGSs) in the presence of hydrophilic functional groups, such as epoxy, carboxyl epoxy, hydroxyl, and sulphonic groups, as well as Stone–Wales and 5-8-5 lattice defects [24]. The chemical functionalization of graphene is a widely accepted technique to improve the dispersibility of graphene in various solvents (aqueous and organic) and polymers [25]. The presence of hydrophilic groups in the chemical modifier facilitates the dispersion of functionalized graphene in water and polar solvents. These advantages of surface functionalized graphene make it an ideal material for sensor and fuel cell applications [26]. Chemically functionalized graphene can be readily mixed with polymers in solution to form a stable dispersion and yield novel types of electrically conductive nanocomposites [27–29]. This new class of nanocomposite materials exhibits good biocompatibility, and could be promising matrices for enzyme immobilization, which would enhance the selectivity and sensitivity of biosensors [30]. Chitosan is an abundant natural biopolymer with excellent film forming ability, biocompatibility, non-toxicity, good water permeability, and high mechanical strength. The combination of nanoparticles with chitosan (CH) has opened up new opportunities for studies of electrochemistry and biosensors [31–33]. These chitosan (CH) and graphene nanocomposite matrices provide the high surface area required to achieve a high loading of enzymes, and a compatible micro-environment to facilitate stability [34–36]. CH also provides favorable contact between the active site of the enzyme and an electrode. One potential drawback of polymer immobilization is that the non-conductive polymer layer forms a diffusion barrier for analytes, and this barrier may decrease the active area of the biosensors, resulting in low sensitivity [37]. The use of biocompatible nanoparticles (NPs) such as gold can successfully overcome these shortcomings related to the use of a non-conductive polymer layer. Moreover, such nanoparticles exhibit electrocatalytic behavior toward hydrogen peroxide (H_2O_2), and have been widely used for sensing applications [38,39]. They are attractive materials for preparing nanoparticle-functionalized graphene, such as AuNPs/SPG nanocomposites, because functionalization may have a synergetic effect on electrocatalytic activity, and thus enhance the sensitivity of the biosensor. Glucose biosensors are a common focus among enzyme-based biosensors due to their importance in the monitoring of blood glucose for the treatment and control of diabetes. Glucose oxidase (GO_x) is employed as the enzyme in most glucose biosensors with various sensing mechanisms. Glucose biosensors have contributed significantly to cancer research (such as that related to the Warburg effect), as well as diabetes and clinical monitoring [40,41].

As part of our ongoing research on the functionalization of graphene sheets and their use in electroanalytical chemistry, we prepared and characterized a hybrid stable nanocomposite of SPG–AuNPs and chitosan-based bionanocomposite film, and demonstrate its application for sensitive glucose sensing. The main advantage of the surface functionalization of graphene via sulfonated polyether–ether–ketone (SPEEK) is to provide more water dispersion ability and to form a stable composite with AuNPs and chitosan for improving biosensing performance [38]. The optimized experimental conditions and real sample testing for the fabrication and operation of the glucose biosensor were established. The fabricated ternary SPG–AuNPs–CH nanocomposite can be used for the detection of glucose in clinical samples, and has many advantages, such as good linearity, high sensitivity, fast response time, good repeatability, reproducibility, and long-term stability.

2. Experimental

2.1. Materials

Natural flake graphite, CH powder (85% deacetylation low molecular weight), $HAuCl_4$ solution, glucose oxidase (Type X-S, from *Aspergillus niger*, GO_x), and β-D(+) glucose were obtained from Sigma-Aldrich, Germany. Potassium permanganate (TCI, Japan), sulfuric acid and sodium borohydrate (Samchun Pure Chemical Co. Ltd., Korea) were used as redox agents. Hydrochloric acid, hydrogen peroxide, ascorbic acid, cholesterol, urea, uric acid, and lactic acid were purchased from Samchun Pure Chemical Co. Ltd., Korea. Hydrazine monohydrate was used as a reducing agent and purchased from TCI, Japan. Polyether–ether–ketone (PEEK) (Victrex 450G, number average molecular weight (M_n) ~ 115,000) was obtained from Victrex plc, UK, and used for the surface modification of graphene after sulfonation. Indium tin oxide (ITO)-coated glass with a sheet resistance of ~15 Ω/cm was used as the substrate for the deposition of the desired nanocomposite used as the working electrode. All phosphate buffer solutions (PBS) were prepared using de-ionized (DI) water.

2.2. Methods

2.2.1. Preparation of gold nanoparticles (AuNPs)

AuNPs were synthesized simply by the chemical reduction of $HAuCl_4$ with $NaBH_4$ at room temperature using a method reported earlier [42], with some modification. In brief, about 0.005 g of $NaBH_4$ was added to 10 mL of DI-water and dissolved completely. Then, 0.1 mL of 0.1 M $HAuCl_4$ aqueous solution was added to 50 mL of DI water and shaken well to mix it homogeneously. The solution of $NaBH_4$ was added dropwise to the $HAuCl_4$ aqueous solution. It was added slowly to prevent aggregation and shaken well in the flask for the addition of each aliquot of reducing agent. The color of the solution changed from yellowish to ruby red, indicating the formation of gold nanoparticles (AuNPs).

2.2.2. Sulfonation of poly(ether–ether–ketone)

The sulfonation of poly(ether–ether–ketone) was done by a method reported earlier [43]. In brief, PEEK pellets (5 g) were dissolved in 100 mL of concentrated H_2SO_4 (95–98 wt%) at room temperature under a nitrogen atmosphere. After the complete dissolution of PEEK in H_2SO_4, it was then stirred vigorously at 55 °C for 5 h. The resulting solution was cooled to room temperature and added to ice-cold DI water. The gray–white precipitate was then washed several times with DI water until the pH became neutral. The product was dried at 70 °C in a vacuum oven to obtain SPEEK. A digital image of the water dispersion of SPEEK at 55 °C is shown in Fig. S1 (supplementary file).

2.2.3. Surface functionalization of graphene using SPEEK

Graphite oxide was prepared by the modified Hummers method [43]. A single layer of graphene oxide (GO) was separated from multilayered graphite oxide by the sonication–centrifugation technique, as reported earlier. The surface modification of graphene using SPEEK was done by a method reported earlier [43]. For surface modification, about 100 mg of SPEEK was dissolved in 50 mL of water at 65–70 °C. SPEEK was highly soluble in water at 65–70 °C. The degree of sulfonation of SPEEK was measured to be 80% [43]. Then, the solution of SPEEK was added to 50 mL of the GO dispersion (1 mg/mL) and stirred for 24 h at 65–70 °C. About 50 μL of hydrazine monohydrate was added and refluxed for 12 h at 100 °C for the reduction of GO. The final product was filtered through cellulose acetate membrane filter paper (0.2-μm pore diameter) to remove

the excess SPEEK and hydrazine monohydrate. The final product was designated as SPEEK-functionalized graphene (SPG).

2.2.4. Preparation of SPG–AuNPs–CH nanocomposite film

One gram of CH powder was added to 100 mL of 0.1 M acetic acid, and the mixture was stirred to form a clear 1 wt% CH solution. The optimal amounts of CH (1 wt%) and SPG (1 mg/mL) (2:1) were mixed, and the mixture was ultra-sonicated for 2 h to obtain a homogeneous dispersion of SPG in the CH matrix. The calculated amount of AuNPs (1 mg/mL) was dispersed in the matrix containing SPG and CH with stirring at room temperature, followed by ultra-sonication for about 2 h to obtain a highly viscous SPG–CH solution with uniformly dispersed AuNPs. A nanocomposite thin film was fabricated by uniformly spreading 15 μL of the SPG–AuNPs–CH nano-biocomposite solution onto an ITO-coated glass surface (0.25 cm^2), and then dried for 12 h at room temperature and washed with de-ionized water to remove any unbound particles. It was found that the optimized ratio of SPG, CH, and AuNPs was 1:2:1, and that 15 μL was the optimum amount of SPG–AuNPs–CH solution, standardized for the dispersion, to deposit onto the ITO surface when preparing the SPG–AuNPs–CH/ITO film, in order to achieve the maximum amperometric current.

2.2.5. Immobilization of GO_x on SPG–AuNPs–CH/ITO nanocomposite film

A freshly prepared solution of GO_x (2 mg/mL) in phosphate buffer solution (50 mM, pH 7.0) was uniformly spread (10 μL) onto a desired SPG–AuNPs–CH/ITO nanocomposite electrode. The GO_x/SPG–AuNPs–CH/ITO bioelectrode was kept undisturbed in a humid chamber for about 24 h at room temperature. This bioelectrode (GO_x/SPG–AuNPs–CH/ITO) was washed thoroughly with phosphate buffer (50 mM, pH 7.0) containing 0.9% NaCl to remove any unbound enzyme, and stored at 4 °C when not in use.

2.3. Characterization

The Raman spectra of SPG were obtained on a Nanofinder 30 (Tokyo Instruments Co., Osaka, Japan). The Fourier transform infrared (FT-IR) spectra of all of the samples were obtained with a Nicolet 6700 spectrometer (Thermo Scientific, USA) over the wavenumber range of 4000–400 cm^{-1}. Transmission electron microscopy (TEM) was carried with a JEM-2200 FS (JEOL, Japan). The field emission scanning electron microscopy (FE-SEM) of SPG and the other samples was carried out on a JSM-6701F (JEOL, Japan). UV–visible spectroscopy was carried out using a UVS-2100 SCINCO spectrophotometer. The cyclic voltammetry (CV), electrochemical impedance spectroscopy (EIS), and amperometric measurements were recorded on a CH660D electrochemical workstation (CH Instruments Inc, USA). The electrochemical measurements were conducted on a three-electrode system with a GO_x/SPG–AuNPs–CH/ITO bioelectrode as the working electrode, a platinum (Pt) wire as the counter electrode, and a saturated Ag/AgCl electrode as a reference electrode in phosphate buffer (50 mM, pH 7.0, 0.9% NaCl) containing 5 mM $[Fe(CN)_6]^{3-/4-}$ as a mediator.

3. Results and discussion

3.1. Structural and morphological studies

The water dispersion stability of SPG is comparable to that of GO due to the presence of hydrophilic group ($-SO_3H$) on the surface of graphene. Fig. S1 (supplementary file) shows the water-dispersion observation of GO, chemically reduced GO, and SPG. In contrast, GO can be homogeneously dispersed in water, forming a brownish dispersion, due to the presence of oxygen functionalities, such as hydroxyl, epoxy, and carboxyl, which interact with the water molecules through hydrogen bonding, leading to the formation of a stable dispersion. However, the water dispersion stability of chemically reduced GO is very poor due to the removal of all the oxygen functionalities from its surfaces and sediments at the bottom of the vial or floating on the top of the water. However, the noncovalently attached SPEEK macromolecules on the surface of graphene confer a hydrophilic nature to the graphene. The presence of hydrophilic functionality ($-SO_3H$ groups in SPEEK) on the surface of graphene helps in the preparation of a stable dispersion of the graphene in an aqueous medium, and can easily prevent the agglomeration of graphene by restacking [43,44].

Raman scattering is a fast and non-destructive technique that provides direct insight into electron–phonon interactions, imparting high sensitivity to electronic and crystallographic structures. It has therefore been extensively applied to the structural investigation of carbon materials, particularly nanotubes. The Raman spectrum of SPG (Fig. 1(a)) exhibits G (graphite) bands at around 1582 cm^{-1} corresponding to the first order scattering of the E_{2g} phonon at the center of the Brillouin zone and 2D band at 2693 cm^{-1} due to the second-order two-phonon mode. The D (diamond) band at 1342 cm^{-1} is due to the out-of-plane breathing mode of the sp^2 atoms of A_{1g} symmetry, which is attributed to local defects and disorder [45,46]. The intensity ratio (I_D/I_G) of the D band to the G band is correlated with the average size of the sp^2 domains. The shape, position, and intensity of the G band relative to those of the D band for this peak depend markedly on the number of layers. The observed ratio of SPG is I_D/I_G = 1.17, indicating the physical adsorption of the SPEEK polymer chains on the surface of graphene. This kind of physical adsorption through π–π interactions precludes the formation of defects due to the surface treatment of graphene. The presence of defects is suitable for biosensor applications. The graphene obtained by chemical vapor deposition does not contain defects, and it is thus not suitable for the amperometric detection of biomolecules. It has been reported that the appropriate chemical functionalization of graphene and the immobilization of biomaterials on it are important, as functional groups can create defects on the surface of graphene [9]. The appearance of a broad peak at 2693 and 2934 cm^{-1} (2D band) indicates the formation of functionalized few-layer graphene [43].

Fig. 1(b) shows an SEM image of SPG, which suggests the formation of a layered structure. The SPG dispersed in water was characterized by TEM. Fig. 1(c) shows the large sheet of SPG, which can be seen on the top of the grid. HR-TEM images were taken to examine the number of layers at multiple locations. The edges of the suspended graphene films on the lacey carbon Cu grid tend to fold back, allowing a cross-sectional view of the films to be obtained. The lateral dimension of the SPG was found to be in the range of 1.8–2 μm. The folding of one or two layers at the edges of the graphene films appears as one or two dark lines, respectively [47]. The appearance of a single dark line in Fig. 1(d) indicates the formation of few-layer graphene.

Fig. S2 (supplementary file) shows the XRD spectra indicating the highly crystalline nature of the as-prepared AuNPs. Five peaks were observed at 38 2°, 44.5°, 64.4°, 77.5°, and 81.7° in the 2θ range of 20–90°, which can respectively be indexed to the (1 1 1), (2 0 0), (2 2 0), (3 1 1), and (2 2 2) reflections of the face-centered cubic structure of metallic gold (JCPDS, card No. 04-0784) [48]. Fig. S3 (supplementary file) shows a typical UV–vis absorption spectrum of the prepared AuNPs. The spectrum exhibits a strong absorption peak around 532 nm. AuNPs exhibit strong absorption that is dependent on the size and shape of particles. For spherical nanoparticles, the absorption band maximum generally falls between about 520 and 532 nm [49]. To further investigate the formation and morphology of the AuNPs, FE-SEM and TEM observations are presented in Fig. S4 (supplementary file). The FE-SEM

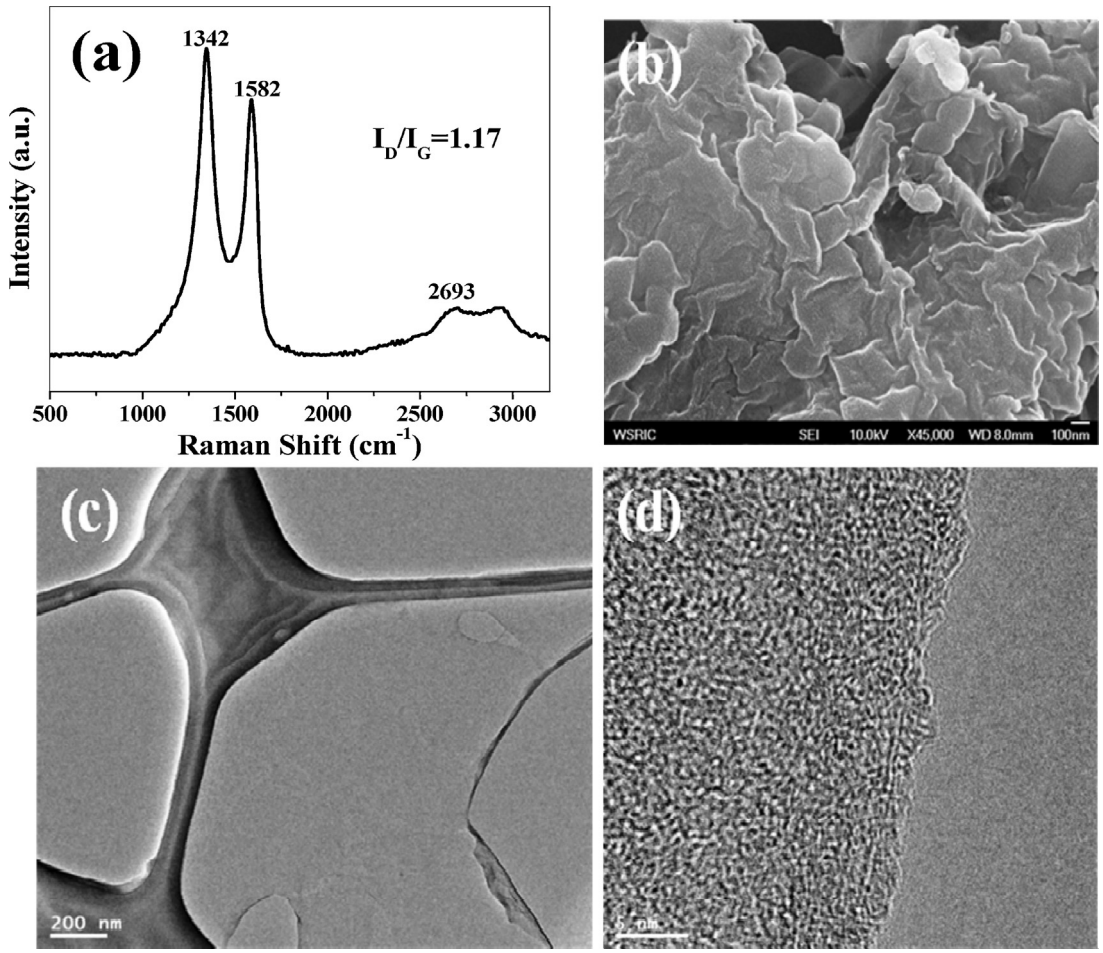

Fig. 1. (a) Raman spectrum (b) SEM image (c) TEM, and (d) HR-TEM images of SPG which confirm the formation of few layers graphene.

and TEM image shows that the AuNPs were uniformly distributed and were predominantly spherical in morphology, with size ranging from 8 to 15 nm with an average size of about 10 ± 3 nm. The AuNPs are generally more chemically stable with high electrocatalytic activity. Nanoparticles can play an important role in the adsorption of biomolecules due to their large specific surface area (surface to volume ratio) and high surface free energy [50]. Jiang et al. studied the effect of nanosized SiO_2 and Au particles on the adsorbability and enzymatic activity of glucose oxidase. They found the amount of adsorbed enzyme increases with decreasing particle size [51]. Yang et al. studied the performance of a glucose biosensor using different sizes of SiO_2 nanoparticles. They found that with decreases in particle size, the response current increased gradually. With a decrease in particle size, the valid surface of the modified electrode is increased, and as the surface enzyme loading increased, more immobilized enzyme could participate in the reaction with glucose and enhance the current response [52].

The FT-IR spectra of the SPG, CH film, SPG–AuNPs–CH/ITO, and GO_x/SPG–AuNPs–CH/ITO bioelectrodes are shown in Fig. 2 in the range of 400–4000 cm^{-1}. The FTIR spectra of SPG (Fig. 2(a)) exhibit broad bands at 3445 cm^{-1} corresponding to O–H stretching due to physically adsorbed water, and the appearance of a peak at 1642 cm^{-1} is due to the sp^2 character of graphite in the functionalized graphene. The peak at 1546 cm^{-1} corresponds to the N–H bending vibration [53]. The appearance of peaks at 1231, 1146, and 678 cm^{-1} confirms the presence of the sulfonic acid groups of SPG [43]. The FTIR spectrum (Fig. 2(b)) of the CH/ITO electrode exhibits the characteristic absorption bands of amino saccharide at 3405 cm^{-1} arising from the overlapping of the –OH and $–NH_2$ bands. The peaks at 2933 and 2880 cm^{-1} are due to the CH_2 stretching, and the peaks at 1640 and 1545 cm^{-1} correspond to the carbonyl stretching (C=O) of the amide I and amide II groups. The peak at 1380 cm^{-1} is assigned to the –C–O stretching mode of the $–CH_2–OH$ groups, and the broad peak at 1065 cm^{-1} is assigned to the β-(1–4) glucosidic band in the polysaccharide unit. Furthermore, the peak at 1066 is attributed to the stretching vibration mode of the hydroxyl group and C–O–C moiety in the glucosamine unit [54]. The FTIR spectra of the SPG–AuNPs–CH/ITO film (Fig. 2(c)) exhibit the characteristic IR bands of the functional group corresponding to SPG–CH, and the additional band found at 463 cm^{-1} indicates the formation of the Au–O–Au gold nanoparticles. Comparing SPG and CH, it is clear that the –C–O–C– epoxy group featured in the range of 1000 to 1200 cm^{-1} becomes a broad band centered at 1075 cm^{-1}, indicating the existence of strong interactions between the AuNPs and epoxy groups [55]. However, the spectrum of the GO_x/SPG–AuNPs–CH/ITO bioelectrode (Fig. 2(d)) shows the broadening of peaks at 3749 and 3435 cm^{-1} due to the addition of the –OH and $–NH_2$ groups of CH and SPG, respectively. The broad band at 1590 cm^{-1} corresponds to the C–N stretching and N–H bending modes of the amide I bands, and that at 1183 cm^{-1} is assigned to the C–O stretching due to the amide bands in the protein, revealing the immobilization of the enzymes onto the SPG–AuNPs–CH/ITO nanocomposite matrix via electrostatic interactions.

The results of the surface morphological studies of the CH/ITO, SPG–CH/ITO electrode, SPG–AuNPs–CH/ITO, and

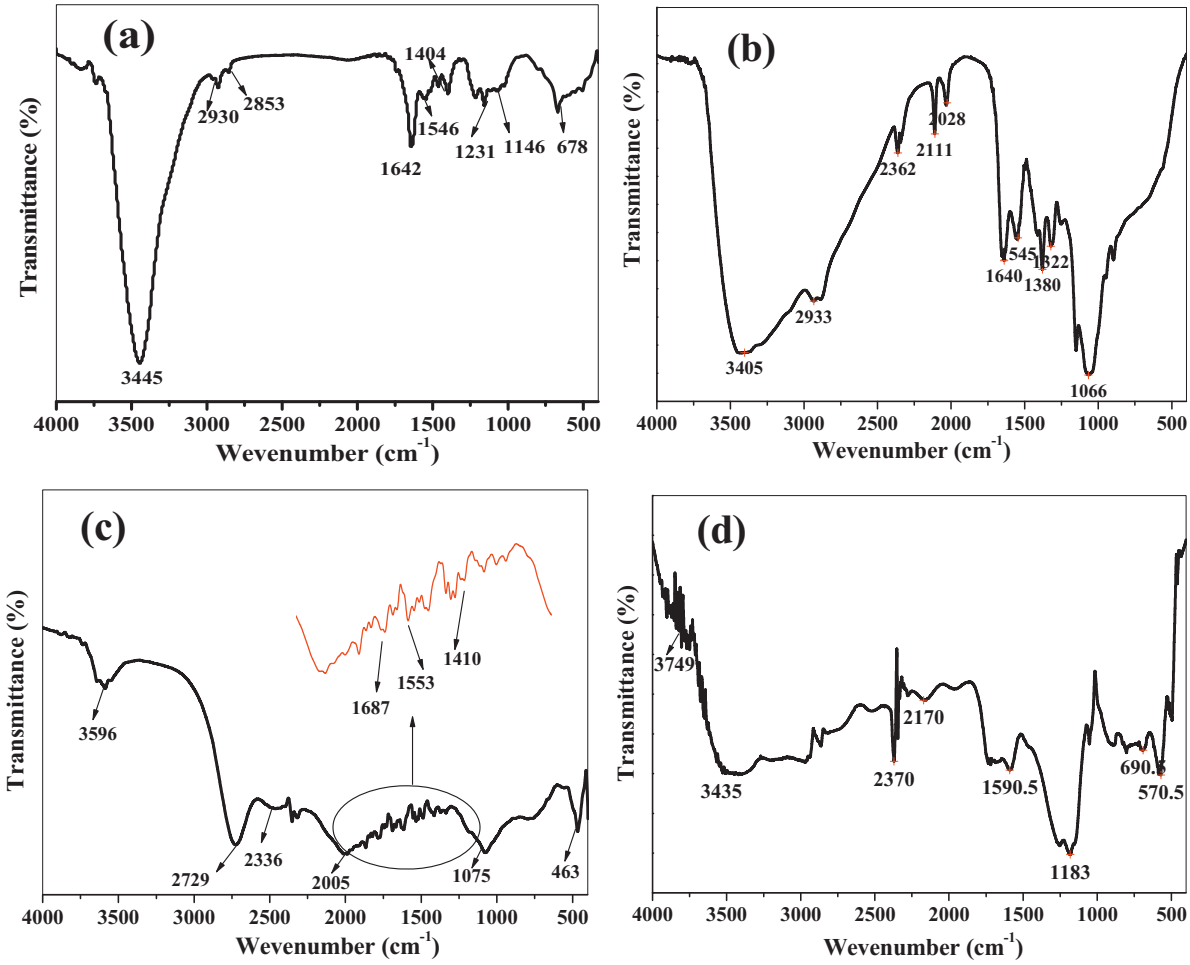

Fig. 2. FTIR spectra of (a) SPG, (b) CH, (c) SPG–AuNPs–CH/ITO nanocomposite film, and (d) GO_x/SPG–AuNPs–CH/ITO bioelectrodes.

GO_x/SPG–AuNPs–CH/ITO bioelectrodes investigated using FE-SEM are shown in Fig. 3. The CH/ITO film (Fig. 3(a)) shows a homogenous and relatively smooth, mesoporous, and crack-free surface. The FE-SEM images of the SPG–CH/ITO composite film (Fig. 3(b)) deposited on the ITO surface reveal the typical crumpled and wrinkled graphene sheet structure on the rough surface of the film. The results indicate that the edge plane of the SPG sheets yields chemical functional groups in the surface modification process, such as $-SO_3H$ and –OH [24], which make them more hydrophilic, and facilitate their interaction with CH, which can increase the effective surface area, thus allowing more AuNPs to be immobilized on the surface of the electrode. As shown in Fig. 3(c), the AuNPs were successfully immobilized on the electrode surface, leading to granular and fibrous nanoporous morphology, and they were embedded uniformly in the SPG–CH matrix with minimum aggregation. It can also be observed in this image that the AuNPs tend to form flower-liked clusters. The inset is a magnified image of an AuNPs cluster, which shows that the diameter of the gold nanoparticles is on the order of ~30 nm. Fig. 3(d) shows the SEM image of the GO_x/SPG–AuNPs–CH/ITO bioelectrodes, clearly demonstrating that GO_x has been immobilized on the electrode surface, because the granular and fibril spherical morphology of SPG–AuNPs–CH/ITO changes into a homogeneous globular porous morphology, due to the ionic interactions. A schematic illustration for the preparation of SPG and the biochemical reaction mechanism of the immobilized GO_x toward glucose on the surface of the SPG–AuNPs–CH/ITO electrode is shown in Fig. 4.

3.2. Electrochemical measurements

3.2.1. Cyclic voltammetric measurements

The electrochemical behavior of GO_x on the modified electrodes was investigated by cyclic voltammetry. Fig. 5(a) shows the cyclic voltammograms of the different electrodes in PBS (50 mM, pH 7.0, 0.9% NaCl) containing $[Fe(CN)_6]^{3-/4-}$ (5 mM) at a scan rate of 30 mV/s. The CV of the bare ITO (curve *i*) exhibits electrochemical characteristics with a couple of redox peaks for the $[Fe(CN)_6]^{3-/4-}$ mediator, and shows an oxidation peak current (*Ipa*) of 0.23 mA. After its modification with CH, the *Ipa* value is enhanced to 0.30 mA (curve *ii*) due to the cationic nature of CH. The peak current of the SPG–CH/ITO electrode (curve *iii*) is higher than those of CH/ITO and bare ITO, which can be ascribed to the excellent conductivity and large surface area of the graphene nanosheets. After the insertion of AuNPs on the surface of the SPG–CH/ITO electrode, the peak current increased up to 0.47 mA (curve *iv*), indicating the good conductivity of the AuNPs. This result might be due to the synergistic effect of graphene and AuNPs [56]. However, the redox peak current obtained with the SPG–AuNPs–CH/ITO electrode is lower than that with the GO_x/SPG–AuNPs–CH/ITO bioelectrode (curve *v*), indicating that the AuNPs can further promote the electron transfer of GO_x due to their good conductivity. Moreover, this response can be attributed to the redox reaction of the electroactive center of the immobilized GO_x [57]. The oxidation peak potential (*Epa*) and reduction peak potential (*Epc*) are located at 0.13 and −0.41 V, respectively. The results of differential pulse voltammetric (DPV)

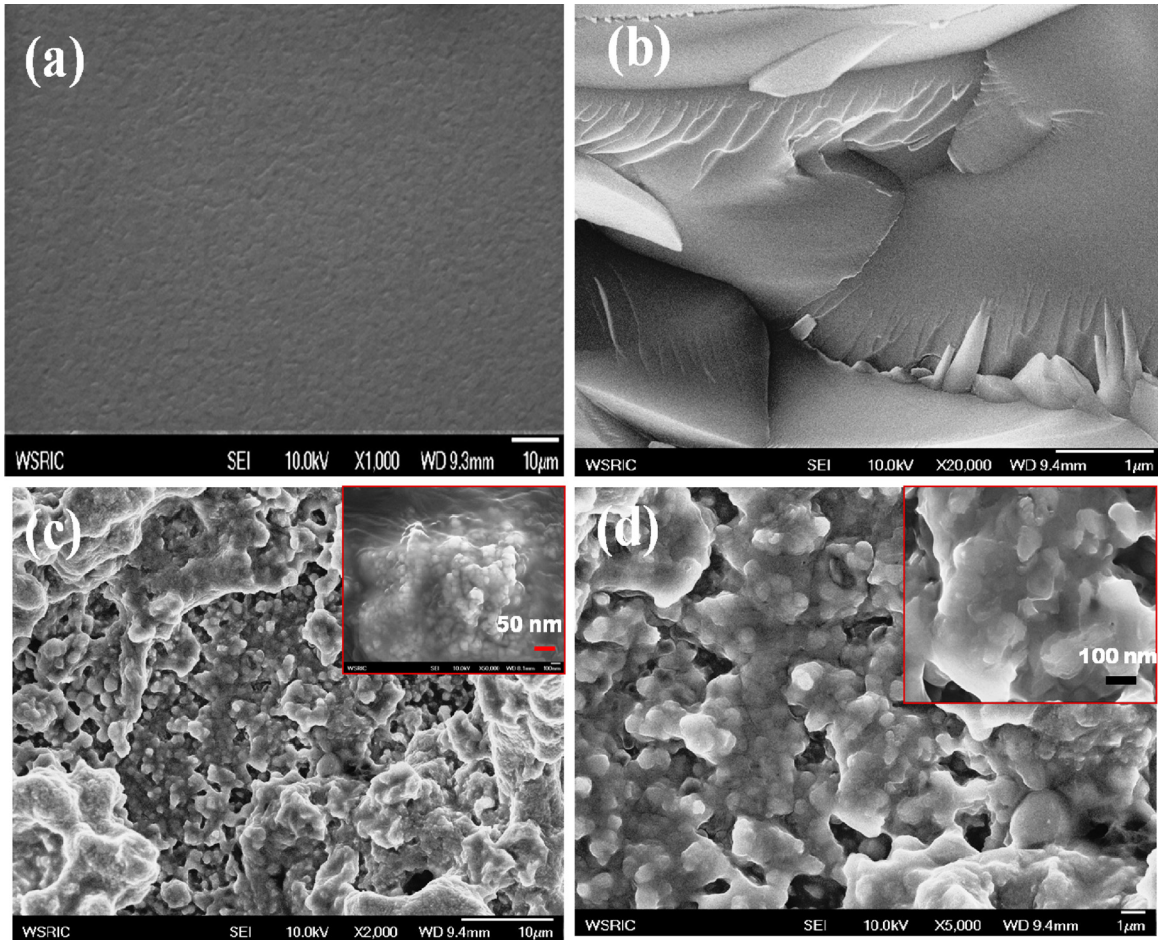

Fig. 3. SEM images of (a) CH/ITO film, (b) SPG–CH/ITO film, (c) SPG–AuNPs–CH/ITO film, and (d) GO_x/SPG–AuNPs–CH/ITO bioelectrodes.

studies reveal similar behavior of the redox potential toward the GO_x/SPG–AuNPs–CH/ITO bioelectrode (Fig. 5(b)).

The influence of the scan rate on the CV performance of the GO_x/SPG–AuNPs–CH/ITO bioelectrode was investigated in PBS (pH 7.0) as a function of the scan rate in the range of 10 to 100 mV/s (Fig. 5(c)). The redox processes of the GO_x/SPG–AuNPs–CH/ITO bioelectrode gave roughly symmetrical anodic and cathodic peaks at relatively slow scan rates. As shown in Fig. 5(d), the magnitudes of the cathodic (*Ipc*) and anodic (*Ipa* peak currents increase linearly with increasing square root of the scan rate ($\upsilon^{1/2}$), indicating typical diffusion-controlled electrochemical behavior, which depends upon the value of the diffusion co-efficient. Moreover, the potential peak shift ($\Delta Ep = Epa - Epc$) also exhibits a linear relationship (with a linear regression co-efficient of 0.9851), for which the scan rate is shown in Fig. S5 (supplementary file). This suggests improved electro-oxidation behavior. All of these characteristics indicate that the redox reaction of GO_x on the SPG–AuNPs–CH film modified electrode is a diffusion-controlled electrochemical process [58,59].

The surface concentration of the electrode can be calculated from the following relation of the Brown–Anson model [34]:

$$I_p = \frac{n^2F^2I * AV}{4RT}$$

where n is the number of electrons transferred (1), F is the Faraday constant (96,485 C/mol), I^* is the surface concentration of the corresponding electrode (mol/cm^2), A is the surface area of the electrode (0.25 cm^2), V is the scan rate (30 mV/s), R is the gas constant (8.314 J/(mol K)), and T is the room temperature (300 K). The surface concentration of the GO_x/SPG–AuNPs–CH/ITO bioelectrodes (8.70×10^{-10} mol/cm^2) is higher than those of the SPG–AuNPs–CH/ITO (6.84×10^{-10} mol/cm^2), SPG–CH/ITO (5.27×10^{-11} mol/cm^2), and bare CH/ITO (4.35×10^{-11} mol/cm^2) electrodes.

3.2.2. Optimization of experimental variables

Influence of pH and working potential: The effect of the solution pH on the electrochemical behavior of the GO_x/SPG–AuNPs–CH/ITO bioelectrode was investigated by CV in PBS (50 mM, pH 7.0, 0.9% NaCl) containing $[Fe(CN)_6]^{3-/4-}$ (5 mM) at a scan rate of 30 mV/s, as shown in Fig. S6 (supplementary file). Fig. 6(a) shows that the redox peak current increases gradually with pH changing from 5.0 to 7.0. The maximum redox peak current is obtained at pH 7.0, and the *Epa* shifted more to its lowest values. When the pH further increases, the redox peak current inversely decreases, and *Epa* is shifted back to higher values. The limited electron transport between the medium and the electrode may lead to a decrease in the electrochemical signal at higher pH (~8.0). These changes in the peak current may arise due to a decrease in concentration of the positively charged moieties present in the matrix (SPG–AuNPs–CH). This could result in decreased interaction between redox ions $[Fe(CN)_6]^{3-/4-}$ and the SPG–AuNPs–CH/ITO nanocomposite surface. Therefore, pH 7.0 was chosen as the optimized condition for further investigation. The effect of the working potential on the performance of the bioelectrode was investigated from 0.1 to 0.8 V in the presence of 100 μL of glucose (5.55 mM) and PBS (50 mM, pH 7.0, 0.9% NaCl) containing 5 mM $[Fe(CN)_6{}^{3-/4-}]$ as a mediator. The steady-state current response clearly increases with increasing working potential from 0.1 to 0.3 V, and then decreases smoothly

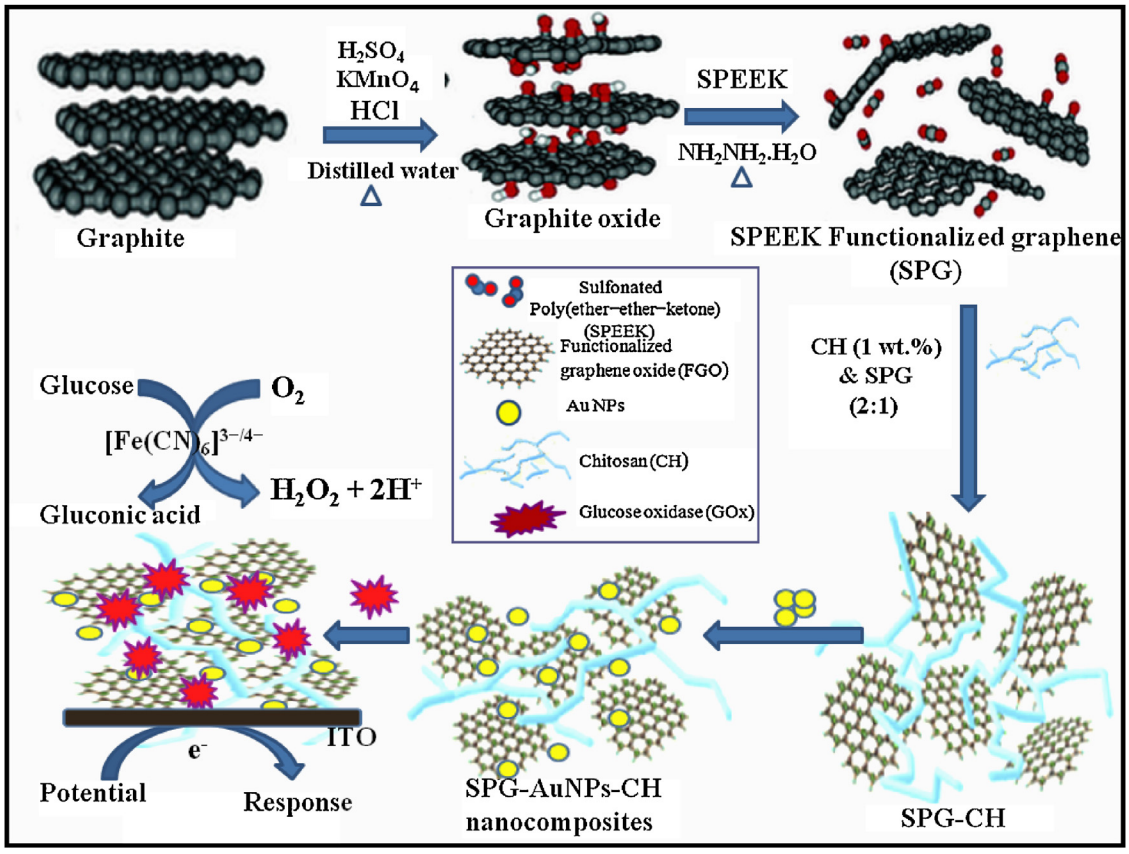

Fig. 4. Schematic illustration for the preparation of SPG and the biochemical reaction mechanism of the immobilized GO_x toward glucose.

from 0.4 to 0.8 V, as shown in Fig. S7 (supplementary file), which is due to the increase of the electron transfer force [60]. A high working potential would cause ascorbic acid and uric acid to be directly oxidized on the electrode surface. In order to avoid this, while obtaining high sensitivity, a working potential of 0.3 V was used.

Further optimization of the experimental conditions such as the amounts of SPG, CH, and AuNPs was maintained in a ratio of 1:2:1, in order to achieve the maximum amperometric current. The effect of the amount of SPG–AuNPs–CH composite solution on the amperometric current response recorded in PBS with 5.6 mM glucose containing $[Fe(CN)_6]^{3-/4-}$ (5 mM) as a mediator at a scan rate of 30 mV/s. The current increases to a value of 0.48 mA, upon raising the nanocomposite amount up to 15 μL, and decreases gradually to 0.42 mA (current) upon increasing the amount to 25 μL. A smaller amount of SPG–AuNPs–CH gives lower sensitivity, possibly due to the decreased loading of enzyme molecules. In addition, the dropping of the current implies that the excess composite may disturb the mass transformation on the surface of the electrode [61,62]. The optimum amount of the composite solution (SPG–AuNPs–CH) used to fabricate the ITO-based bioelectrode was 15 μL (supplementary file, Fig. S8). The GO_x loading was also found to have a substantial effect on the amperometric response of the biosensor toward 5.6 mM glucose (supplementary file, Fig. S9). The maximum current was obtained at 2 mg/mL of GO_x loading. Therefore, 2 mg/mL of GO_x was adopted to fabricate the biosensor.

3.2.3. Amperometric response studies of GO_x/SPG–AuNPs–CH/ITO bioelectrode

The cyclic voltammograms of the fabricated GO_x/SPG–AuNPs–CH/ITO bioelectrode have been investigated as a function of the glucose concentration (0–22.2 mM) in PBS (50 mM, pH 7.0, 0.9% NaCl) containing $[Fe(CN)_6]^{3-/4-}$ (5 mM) as a mediator at a scan rate of 30 mV/s in N_2 atmosphere. The working mechanism of the glucose biosensor during measurements could be explained by taking into account the dual role of GO_x, which provides not only good specificity, but also works as a catalyst to initiate the chemical reaction. The reaction scheme is as follows:

$$\text{glucose} + GO_x(\text{oxi}) \rightarrow \text{gluconicacid} + GO_x \quad (\text{red})$$

$$GO_x(\text{red}) + Fe^{3+}(\text{ferricynide}) \rightarrow GO_x(\text{oxi}) + Fe^{2+} \quad (\text{ferrocynide})$$

$$Fe^{2+}(\text{ferrocynide}) \rightarrow Fe^{3+}(\text{ferricynide}) + e^- \quad (\text{atelectrode})$$

However, there is no oxidation peak related to the generation of H_2O_2 (usually obtained at 0.05 V). However, when a mediator ($K_3[Fe(CN)_6]$) is present in the electrolyte, the electron transfer takes place through the mediator at a low potential of 0.12 V, as observed in the present case. The schematic of the reaction in the presence of mediator ($K_3[Fe(CN)_6]$) is shown in Fig. S10 (supplementary file).

Fig. 6(b) displays the typical amperometric responses of the GO_x/SPG–AuNPs–CH/ITO bioelectrode in PBS (50 mM, pH 7.0, 0.9% NaCl) containing $[Fe(CN)_6]^{3-/4-}$ (5 mM) as a redox couple for varying the concentration of glucose. The peak oxidation current continues increasing with the successive addition of glucose from 0 to 22.2 mM. This may be due to the fact that conductive SPG and AuNPs act as good receptors of the electrons generated during the reoxidation of GO_x and transferred to the electrode via Fe^{3+}/Fe^{2+} conversion, resulting in an increased electrochemical response. As the concentration of glucose in the electrolyte solution increases, a greater number of electrons are generated, resulting in enhanced peak oxidation and reduction currents for the GO_x/SPG–AuNPs–CH/ITO bioelectrode. The enzyme electrode

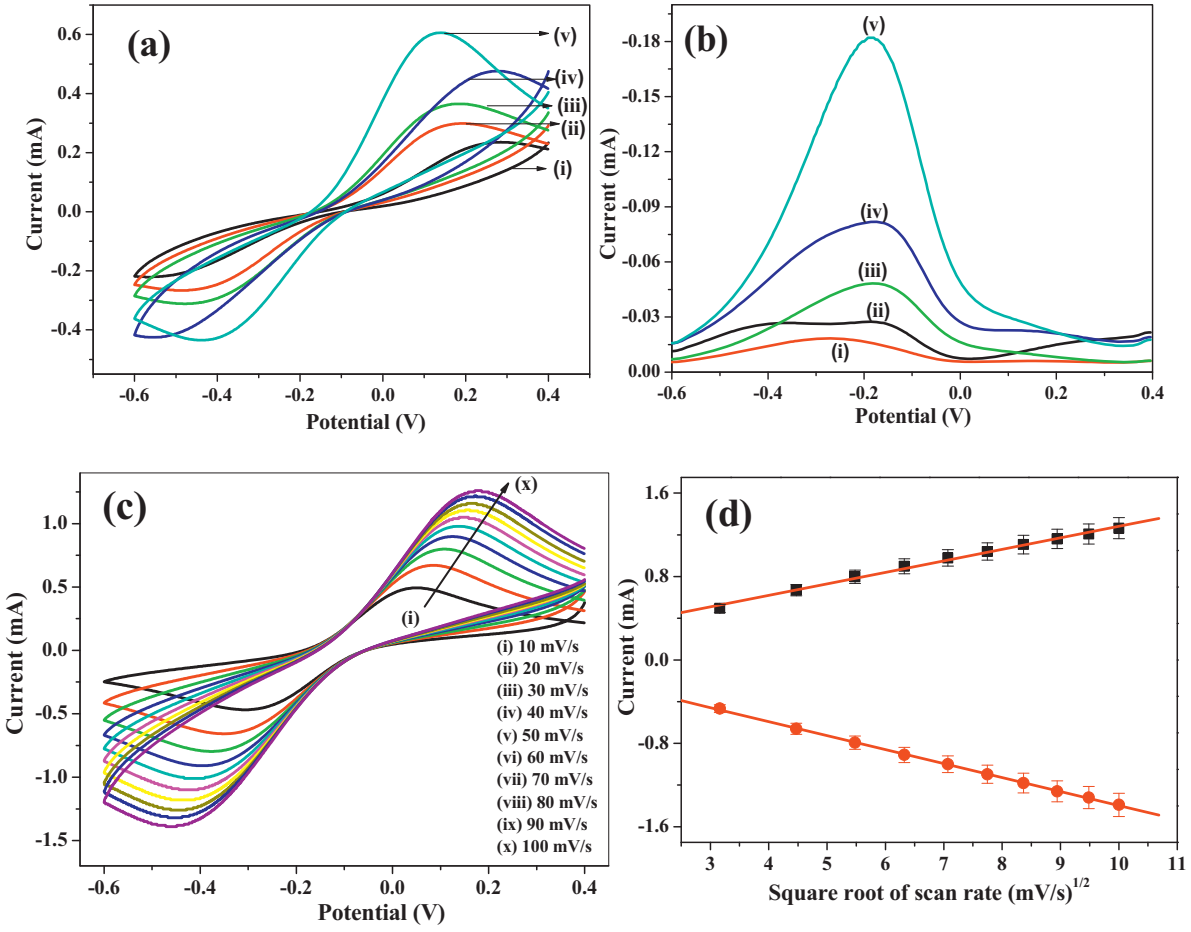

Fig. 5. (a) CV, (b) DPV of (i) bare ITO electrode, (ii) CH/ITO film, (iii) SPG–CH/ITO film, (iv) SPG–AuNPs–CH/ITO film, and (v) GO_x/SPG–AuNPs–CH/ITO bioelectrodes, (c) CV of GO_x/SPG–AuNPs–CH/ITO bioelectrode with increasing scan rate from 10 to 100, (d) shows magnitude of potential difference as a function of scan rate (10–100 mV/s).

exhibits excellent electrocatalytic activity for glucose detection with steep increases in current responses, and the time required to reach 96% of the steady-state current is within 10 s. This result indicates that the biosensor shows very sensitive and rapid response characteristics. This might be due to the fact that SPG nanosheets are highly electronconductive, which provides a low-resistance pathway between glucose and the immobilized GO_x, facilitating the electron transfer and reducing the response time.

The calibration curve (Fig. 6(c)) corresponding to the amperometric response current shows a linear variation with increasing concentration of glucose in the range of 0.26 to 22.2 mM (R = 0.992) at 0.12 V, and from reduction current (R = 0.999) at −0.38 V. However, the calibration curve corresponds to the plot of the electrochemical response vs. the glucose concentration. This figure shows that this sensor shows a wide linear range of glucose concentration from 0.5 to 22.2 mM. The limit of detection has been evaluated using $3\sigma/m$ criteria, where σ is the standard deviation, and m is the slope of the calibration plot. The limit was found to be 0.13 mM based on three times the signal-to-noise ratio. This sensitivity of the biosensor might be due to its large surface area, the fast electron transfer activity of SPG, and the electrocatalytic synergy resulting from the AuNPs and graphene. Within the nanocomposite, GO_x can contact both SPG and the AuNPs, which would allow fast electron transfer with a relatively low barrier between the enzyme and the electrode. The sensitivity of the fabricated GO_x/SPG–AuNPs–CH/ITO bioelectrode was calculated from the slope of the curve and found to be 6.51 μA/(mM cm^2). The standard deviation and limit of detection for the bioelectrode were found to be 3.7 μA and 0.13 mM, respectively. Therefore, this GO_x/SPG–AuNPs–CH/ITO bioelectrode can be employed as a glucose sensor. It is well known that the diabetic glucose concentration is above 6.7 mM [63], which indicates that this biosensor is suitable for the determination of human blood-sugar concentration.

Fig. S11 (supplementary file) shows the chronoamperometry response of the GO_x/SPG–AuNPs–CH/ITO bioelectrode as a function of the glucose concentration (0–22.2 mM) in PBS (50 mM, pH 7 0, 0.9% NaCl) containing $[Fe(CN)_6]^{3-/4-}$ (5 mM) as a mediator at a scan rate of 30 mV/s. The results indicate that an increase in the concentration of glucose was accompanied by an increase in the anodic current obtained for a potential step of 30 mV/s. The inset of Fig. S11 shows the calibration curve of the chronoamperometric current response for sampling at a fixed time as a function of glucose concentration. The response is linearly proportional to the concentration of glucose in the range of 0–22.2 mM with R = 0.9848. The choronoamperometric measurements and calibration curve for different glucose concentrations supported the results obtain by cyclic voltammetry response studies.

The value of the enzyme–substrate kinetic parameter (Michaelis–Menten constant, K_m) for the GO_x/SPG–AuNPs–CH/ITO bioelectrode was found to be 1.96 mM using the Hanes plot (Fig. 6(d)), which is a graph of the substrate concentration versus the substrate concentration/current (Fig. 6(d)). This small K_m value indicates the increased affinity of the GO_x/SPG–AuNPs–CH/ITO bioelectrode, which is attributed to the favorable conformation of the enzymes, their higher loading onto the AuNP-modified SPG/CH electrode surface and the efficient maintenance of the enzymatic activity. The value of K_m depends on various factors, such as the matrix and the method of immobilizing the enzymes,

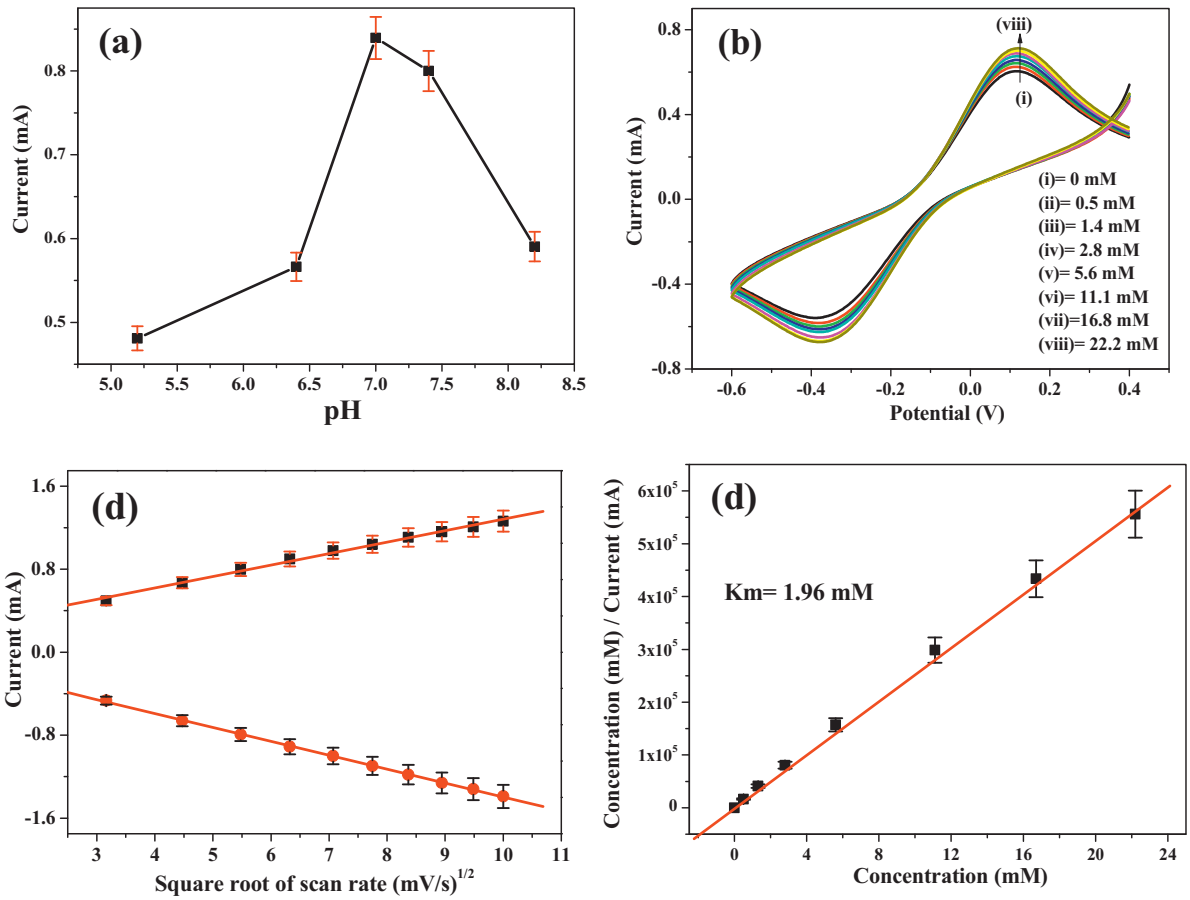

Fig. 6. (a) Change of the conjugative current response as a function of pH from 8.2 to 5.7 in phosphate buffer (50 mM, pH 7.0, 0.9% NaCl) containing 5 mM $[Fe(CN)_6]^{3-/4-}$ toward 5.6 mM glucose solution. (b) Electrochemical response of GO_x/SPG–AuNPs–CH/ITO bioelectrode with respect to the glucose concentration (0–22.2 mM) in phosphate buffer (50 mM, pH 7.0, 0.9% NaCl) containing 5 mM $[Fe(CN)_6]^{3-/4-}$ at a scan rate of 30 mV/s, (c) Shows the calibration curves for the variation in current as a function of the glucose concentration and (d) Hanes plot between the substrate concentration and substrate concentration/current.

which could bring about different conformational changes in the enzyme structure, as the kinetics of the enzyme is sensitive to the environment [54]. This good performance can be explained by the composite nanosheets not only providing SPG with such remarkable electrical conductivity with CH as a redox probe, but also supplying an interface of abundant amino-groups to assemble AuNPs for GO_x, which improved the sensitivity and selectivity of the biosensor.Additionally, the biospecific interactions between the enzyme and SPG–AuNPs–CH/ITO electrode increase the quantity of GO_x immobilized on the electrode. All of these factors cause the biosensor to possess good bioactivity, high sensitivity, and good selectivity.

3.2.4. *Interference, stability and reproducibility of the biosensor*

The influence of common interferents on the fabricated GO_x/SPG–AuNPs–CH/ITO bioelectrode was determined in PBS (50 mM, pH 7.0, 0.9% NaCl) containing $[Fe(CN)_6]^{3-/4-}$ (5 mM) at a scan rate of 30 mV/s using the CV technique shown in Fig. S12 (supplementary file). The change in electrochemical current response was measured in PBS containing equal amounts (1:1) of standard glucose (5.6 mM) solution along with a normal physiological concentration of common interferents such as glucose (5 mM), ascorbic acid (0.05 mM), lactic acid (0.5 mM), urea (1 mM), and uric acid (0.1 mM). The bar graph (Fig. 7(a)) shows that the values of the oxidation peak current decrease by 3% in cholesterol and uric acid, and by 1% in lactic acid and the mixture of all interferents. It is clear that the interference effect in the presence of ascorbic acid and urea is negligible. We detected glucose based on the consumption of oxygen, and the potential was selected to be less than −0.30 V. However, the signal of AA began after −0.1 V. These results indicate that the response of the GO_x/SPG–AuNPs–CH/ITO bioelectrode is not significantly affected by the presence of these interferents.

As shown in Fig. 7(b), the GO_x/SPG–AuNPs–CH/ITO nanocomposite film modified electrode reached 96% of the steady-state current within 10 s. This fast response can be attributed to the AuNPs, which not only provide a high surface area and excellent electrical conductivity, but also improve the electrocatalytic activity, thus allowing for the rapid electro-oxidation of H_2O_2. The thin and highly porous structure of the SPG–CH matrix also contributes by facilitating fast substrate diffusion.

The reproducibility of the proposed glucose biosensor was studied. Repetitive measurements were carried out in 10 mL of PBS containing 5.6 mM glucose solution. The response current of the modified electrode was changed by 4.5% from its initial response after being stored in a refrigerator at 4 °C for two weeks. The relative standard deviation (RSD) of the current response to 5.6 mM glucose was 3.6% for 10 successive measurements, which proved that the biosensor also had good reproducibility.

The shelf-life of the fabricated GO_x/SPG–AuNPs–CH/ITO bioelectrode Fig. 7(c) was monitored by conducting amperometric measurements in the presence of 5.6 mM standard glucose solution in PBS at regular intervals of 1 day for up to 15 days, and then for a further interval of 15 days. It was found that the bioelectrode retains its enzyme activity and up to 94% of the current magnitude after 15 days, 91% after 30 days, 88% after 45 days, and 83% after 60 days, showing a longer lifetime when stored under

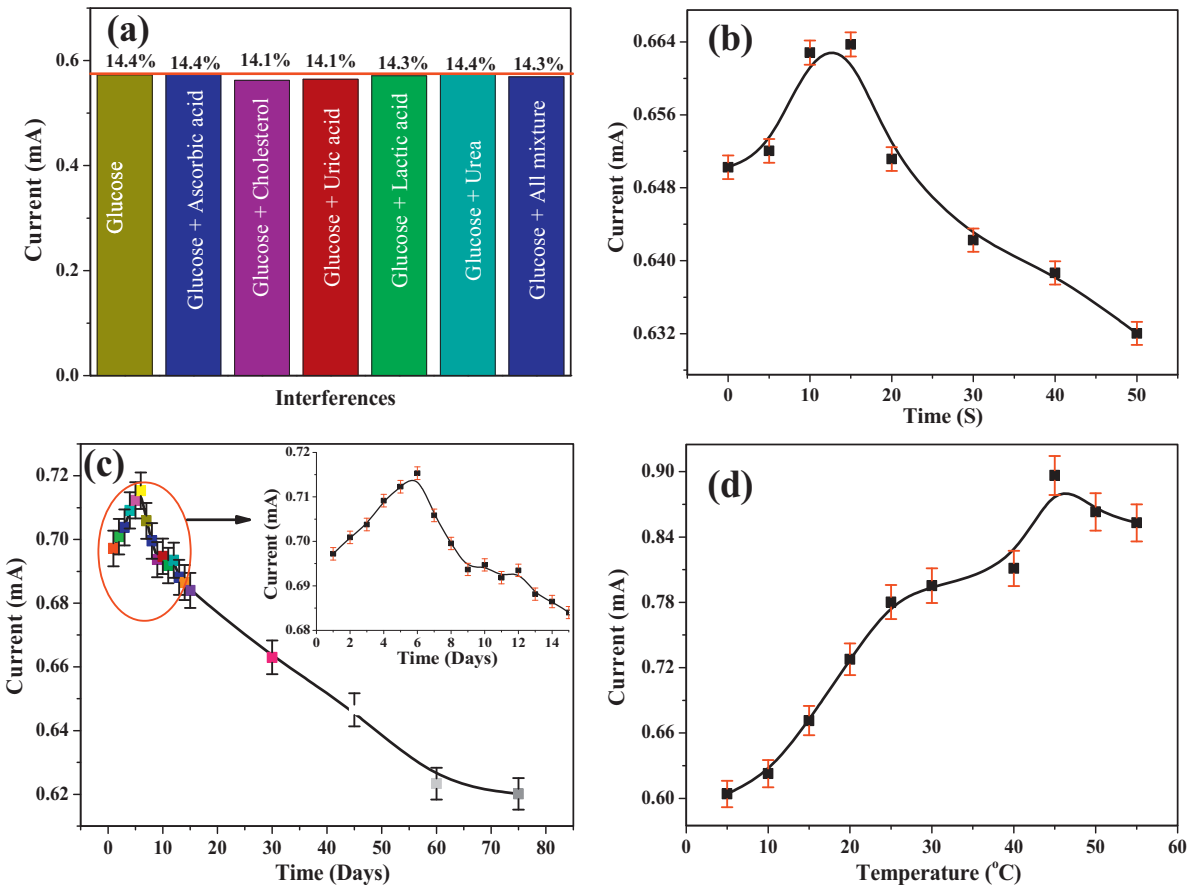

Fig. 7. (a) Bar graph for the effects of different interferents on the electrochemical response of the GO_x/SPG–AuNPs–CH/ITO bioelectrode, (b) electrochemical response time during the incubation period from 5 to 60 s, (c) shelf-life curve for GO_x/SPG–AuNPs–CH/ITO bioelectrode as a function of the number of days, (d) effect of temperature on GO_x/SPG–AuNPs–CH/ITO bioelectrode from 10 to 60 °C.

refrigerated conditions (4 °C). This good stability may be due to the fact that the stable SPG–AuNPs–CH matrix provides an appropriate microenvironment for retaining the bioactivity of the enzyme molecules.

3.2.5. Effect of temperature

The temperature of the medium is also an important parameter for the enzyme activity. The effect of temperature on the amperometric response was also investigated in the presence of 5.6 mM standard glucose solution in PBS in the range of 5–60 °C, and the results are shown in Fig. 7(d). The response increased with increasing temperature, reached a maximum at 45 °C, and subsequently decreased. This might be due to the denaturation or leaching of the immobilized enzyme. A temperature of 25 °C (room temperature) was chosen for all further experiments. Table 1 contains the performance of some glucose biosensors based on graphene reported in the literature, along with their important parameters [27,30,38,58,64–69].

3.2.6. Human serum sample analysis

In order to demonstrate the practical usage of the biosensor, blood serum samples were assayed. The blood serum samples and their glucose concentrations were provided by a local medical examination center located in Jeonju, Korea. The electrochemical response current was measured in both the blood serum and a standard sample in the presence of PBS (50 mM, pH 7.0, 0.9% NaCl) containing $[Fe(CN)_6]^{3-/4-}$ (5 mM) at a scan rate of 30 mV/s. The original glucose concentration of the blood serum sample was

Table 1
Construction and performance of some glucose biosensors reported in literature, along with their important parameters based on graphene nanomaterials (as one of the component in the matrix for enzyme immobilization).

S No.	Glucose biosensor	Protocol	Linear range (mM)	Detection limit (μM)	Sensitivity (μA/mM/cm^2)	K_m value (mM)	Shelf life	Referenecs
1	GOD/Pt/FGS/chitosan/GCE	Electrodeposition	Sub-μM to 5 mM	0.6	–	–	–	[27]
2	GOD/GR/CS/GC	Drop-coating	0.08–12	20	37.93	4.4	–	[30]
3	GOD/AuNPs/GR/CS/Au	Drop-coating	2–14	180	0.55	–	30 days	[38]
4	GOD/GR/PFIL/GC	Drop-coating	2–14	–	–	–	2 weeks	[58]
5	GOD/PdNPs/CS–GR/GC	Cross linking	0.001–1	0.2	31.2	1.2	2 weeks	[64]
6	GCE/RGO–PAMAM–Ag	Drop-coating	0.032–1.89	4.5	75.72	9.6	–	[65]
7	GCE/GP–GOD	Drop casting	2–22	20	–	–	–	[66]
8	GO_x/CMG–IL/Au	Drop casting	1–6	0.376	0.64	–	2 weeks	[67]
9	GCE/TiO2–GR/GOD	Drop casting	0–8	–	6.2	–	100 cycle	[68]
10	GOD/Pd/RGO/GCE	Cross linking	0–4	0.34	14.1	0.057	2 weeks	[69]
11	GO_x/SPG–AuNPs–CH/ITO	Drop casting	0.5 to 22.2	510	6.51	1.96	70 days	Present work

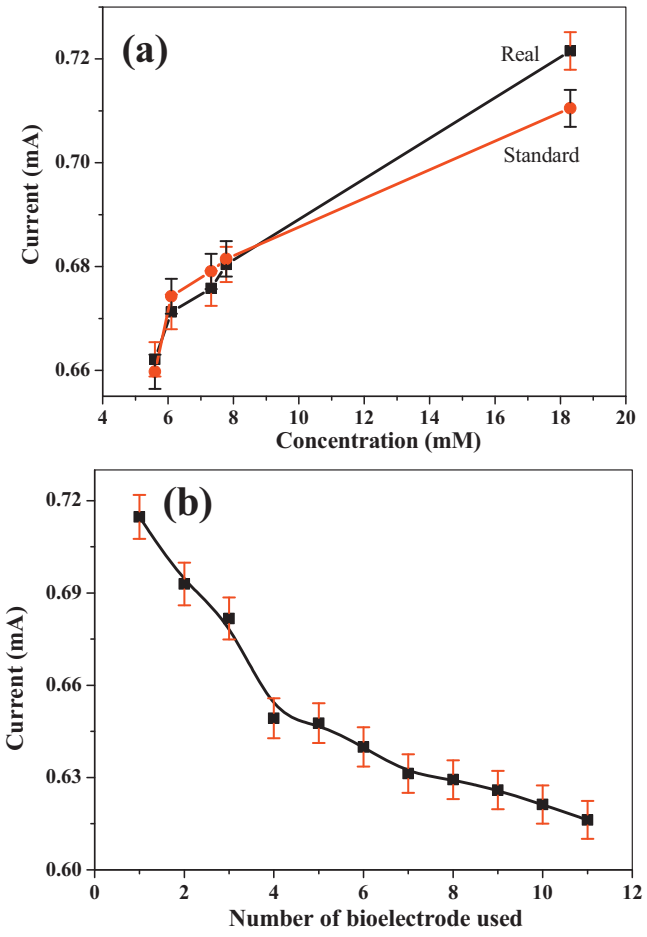

Fig. 8. (a) Determination of glucose concentration; in serum sample and in prepared standard sample. (b) Reusability of the GO_x/SPG–AuNPs–CH/ITO bioelectrode for the estimation of glucose (7.3 mM) in real sample.

hypothesized as 5 mM, and the electrolyte solution used for the CV experiment was a mixed solution containing the same volumes of blood serum and PBS. The magnitude of the current increases linearly with increasing glucose concentration ($R = 0.981$), and the blood serum samples and prepared standard glucose solution were in reasonable agreement with each other (Fig. 8(a)), indicating that the fabricated biosensor can be used for the precise determination of the blood glucose concentration in real clinical samples. As shown in Table 2, the results were satisfactory, and agreed closely with those measured by our reduction method, which can eliminate the interference of other molecules in the blood, making it a promising candidate to determine the blood sugar concentration in practical clinical analysis with relative standard deviations ranging from 0.5 to 5.0%. Fig. 8(b) shows the reusability of the fabricated GO_x/SPG–AuNPs–CH/ITO bioelectrodes for the estimation of glucose in the real sample (7.3 mM). The results indicate that the prepared bioelectrode can be reused for up to 11 cycles with a 14% loss of response current.

Table 2
Determination of glucose in serum sample.

Glucose concentration (mM)	Current value obtained from serum sample (mA)	Current value obtained from pure glucose sample (mA)	% RSD
18.3	0.72	0.71	2.20
7.7	0.68	0.68	0.21
7.3	0.68	0.68	0.65
6.1	0.67	0.67	0.61
5.5	0.66	0.66	0.47

4. Conclusion

We have successfully prepared an AuNPs-decorated water-dispersible functionalized graphene/chitosan nanocomposite, and have characterized it by SEM, TEM, and Raman spectroscopy. The prepared SPG–CH/AuNPs nanocomposite has been utilized for the fabrication of a glucose biosensor by immobilizing GO_x. The fabricated biosensor had a sensitivity of 6.51 μA/(mM cm^2), a broad linear range of 0.5 to 22.2 mM, a limit of detection of 0.13 mM, and fast response time of 10 s. This amperometric performance was attributed due to the large area, the excellent catalytic activity and high conductivity of SPG, the good biocompatibility and film-forming ability of chitosan, and the excellent conductivity and catalytic activity of the AuNPs. The fabricated bioelectrode showed good repeatability for more than 15 cycles and long-term stability for up to 70 days with a decrease of the current response by 16% compared to its original response. The synergistic effect between graphene and the AuNPs may promote the electrocatalytic activity toward the electrolyte on the electrode surface. Moreover, the fabricated bioelectrode is thermally stable, exhibiting a negligible interference effect, thus allowing it to be used for the clinical analysis of real blood serum samples. The ternary SPG–CH/AuNPs nanocomposite may offer a new approach for developing novel types of highly sensitive and stable electrochemical biosensors.

Acknowledgments

This study was supported by the Basic Science Research Program (NRF-2013R1A1A2011608) and the Converging Research Center Program (2012K001428) through the National Research Foundation of Korea (NRF) funded by the Ministry of Education, Science and Technology and by the Ministry of Science, ICT & Future Planning of Korea.

Appendix A. Supplementary data

Supplementary data associated with this article can be found, in the online version, at http://dx.doi.org/10.1016/j.procbio.2013.07.025.

References

[1] Novoselov KS, Jiang Z, Zhang Y, Morozov SV, Stormer HL, Zeitler U, et al. Room-temperature quantum Hall effect in graphene. Science 2007;315(1517):1379.
[2] Singh V, Joung D, Zhai L, Das S, Khondaker SI, Seal S. Graphene based materials: past, present and future. Prog Mater Sci 2011;56:1178–271.
[3] Wang X, Zhi LJ, Mullen K. Transparent, conductive graphene electrodes for dye-sensitized solar cells. Nano Lett 2008;8:323–7.
[4] Vivekchand SRC, Rout CS, Subrahmanyam KS, Govindaraj A, Rao CNR. Graphene-based electrochemical supercapacitors. J Chem Sci 2008;120:9–13.
[5] Hu N, Wang Y, Chai J, Gao R, Yang Z, Kong ES, Zhang Y. Gas sensor based on *p*-phenylenediamine reduced graphene oxide. Sens Actuators, B: Chem 2012;163:107–14.
[6] Ang PK, Chen W, Wee ATS, Loh KP. Solution-gated epitaxial graphene as pH sensor. J Am Chem Soc 2008;130:14392–3.
[7] Wang Y, Li YM, Tang LH, Lu J, Li JH. Application of graphene-modified electrode for selective detection of dopamine. Electrochem Commun 2009;11:889–92.
[8] Shao Y, Wang J, Wu H, Liu J, Aksay IA, Lin Y. Graphene based electrochemical sensors and biosensors: a review. Electroanalysis 2010;22:1027–36.
[9] Kuila T, Bose S, Khanra P, Mishra AK, Kim NH, Lee JH. Recent advances in graphene-based biosensors. Biosens Bioelectron 2011;26:4637–48.
[10] Stankovich S, Dikin DA, Dommet GHB, Kohlhaas KM, Zimney EJ, Stach EA, et al. Graphene-based composite materials. Nat Lett 2006;442:282–6.
[11] Kim K, Park HJ, Woo BC, Kim KJ, Kim GT, Yun WS. Electric property evolution of structurally defected multi-layer graphene. Nano Lett 2008;8:3092–6.
[12] Lee C, Wei XD, Kysar JW, Hone J. Measurement of the elastic properties and intrinsic strength of monolayer graphene. Science 2008;321:385–8.

[13] Chen H, Müller MB, Gilmore KJ, Wallace GG, Li D. Mechanically strong, electrically conductive, and biocompatible graphene paper. Adv Mater 2008;20:3557–61.
[14] Segal M. Small start-up companies are making large volumes of graphene, the world's thinnest material, for applications such as composites and electrodes. Nat Nanotechnol 2009;4:612–4.
[15] Bunch JS, Van der Zande AM, Verbridge SS, Frank IW, Tanenbaum DM, Parpia JM, et al. Electromechanical resonators from graphene sheets. Science 2007;315:490–3.
[16] Chua CK, Ambrosi A, Pumera M. Graphene based nanomaterials as electrochemical detectors in lab-on-a-chip devices. Electrochem Commun 2011;13:517–9.
[17] Parlak O, Tiwari A, Turner AP, Tiwari A. Template-directed hierarchical self-assembly of graphene based hybrid structure for electrochemical biosensing. Biosens Bioelectron 2013;45:53–62.
[18] Tiwari A, Ramalingam M, Kobayashi H, Turner AP. Biomedical materials and diagnostic devices. USA: Wiley-Scrivener; 2012.
[19] Zuo X, He S, Li D, Peng C, Huang Q, Song S, Fan C. Graphene oxide-facilitated electron transfer of metalloproteins at electrode surfaces. Langmuir 2010;26:1936–9.
[20] Kim J, Piao Y, Hyeon T. Multifunctional nanostructured materials for multimodal imaging, and simultaneous imaging and therapy. Chem Soc Rev 2009;38:372–90.
[21] Nel AE, Mädler L, Velegol D, Xia T, Hoek EMV, Somasundaran P, et al. Understanding biophysicochemical interactions at the nano–bio interface. Nat Mater 2009;8:543–57.
[22] Zhang Y, Wang Y, Jia J, Wang J. Nonenzymatic glucose sensor based on graphene oxide and electrospun NiO nanofibers. Sens Actuators, B: Chem 2012;17:1–172, 580-7.
[23] Kuila T, Bose S, Mishra AK, Khanra P, Kim NH, Lee JH. Chemical functionalization of graphene and its applications. Prog Mater Sci 2012;57:1061–105.
[24] Schniepp HC, Li JL, McAllister MJ, Sai H, Herrera-Alonso M, Adamson DH, et al. Functionalized single graphene sheets derived from splitting graphite oxide. J Phys Chem B 2006;110:8535–9.
[25] Shan C, Yang H, Han D, Zhang Q, Ivaska A, Niu L. Water-soluble graphene covalently functionalized by biocompatible poly-L-lysine. Langmuir 2009;25:12030–3.
[26] Wang D, Choi D, Li J, Yang Z, Nie Z, Kou R, et al. Self-assembled TiO_2–graphene hybrid nanostructures for enhanced Li–ion insertion. ACS Nano 2009;3:907–14.
[27] Wu H, Wang J, Kang X, Wang C, Wang D, Liu J, et al. Glucose biosensor based on immobilization of glucose oxidase in platinum nanoparticles/graphene/chitosan nanocomposite film. Talanta 2009;80:403–6.
[28] Li D, Kaner RB. Graphene-based materials. Science 2008;320:1170–1.
[29] Xu Y, Bai H, Lu GW, Li C, Shi GQ. Flexible graphene films via the filtration of water-soluble noncovalent functionalized graphene sheets. J Am Chem Soc 2008;130:5856–7.
[30] Kang X, Wang J, Wu H, Aksay IA, Liu J, Lin Y. Glucose oxidase–graphene–chitosan modified electrode for direct electrochemistry and glucose sensing. Biosens Bioelectron 2009;25:901–5.
[31] Tiwari A, Terada D, Sharma PK, Parashar V, Yoshikawa C, Pandey AC, Kobayashi H. An ultra sensitive saccharides detection assay using carboxyl functionalized chitosan containing Gd_2O_3: Eu^{3+} nanoparticles probe. Anal Methods 2011;3:217–26.
[32] Tiwari A, Gong S. Electrochemical study of chitosan–SiO_2–MWNT composite electrodes for the fabrication of cholesterol biosensors. Electroanalysis 2008;20:2119–26.
[33] Solanki PR, Kaushik A, Ansari AA, Tiwari A, Malhotra BD. Multi-walled carbon nanotubes/sol–gel-derived silica/chitosan nanobiocomposite for total cholesterol sensor. Sens Actuators, B: Chem 2009;137:727–35.
[34] Singh J, Kalita P, Singh MK, Malhotra BD. Nanostructured nickel oxide–chitosan film for application to cholesterol sensor. Appl Phys Lett 2011;98:123702.
[35] Liu Y, Wang MK, Zhao F, Xu ZA, Dong SJ. The direct electron transfer of glucose oxidase and glucose biosensor based on carbon nanotubes/chitosan matrix. Biosens Bioelectron 2005;21:984–8.
[36] Kang XH, Mai ZB, Zou XY, Cai PX, Mo JY. J Nanosci Nanotechnol 2007;7:1618–24.
[37] Shi J, Cha TG, Claussen JC, Diggs AR, Choi JH, Porterfield DM. Microbiosensors based on DNA modified single-walled carbon nanotube and Pt black nanocomposites. Analyst 2011;136:4916–24.
[38] Shan C, Yang H, Han D, Zhang Q, Ivaska A, Niu L. Graphene/AuNPs/chitosan nanocomposites film for glucose biosensing. Biosens Bioelectron 2010;25:1070–4.
[39] Ge S, Yan M, Lu J, Zhang M, Yu F, Yu J, et al. Electrochemical biosensor based on graphene oxide–Au nanoclusters composites for L-cysteine analysis. Biosens Bioelectron 2012;31:49–54.
[40] McLamore ES, Shi J, Jaroch D, Claussen JC, Uchida A, Jiang Y, et al. A self referencing platinum nanoparticle decorated enzyme-based microbiosensor for real time measurement of physiological glucose transport. Biosens Bioelectron 2011;26:2237–45.
[41] Jiang Y, Zhang Q, Li F, Niu L. Glucose oxidase and graphene bionanocomposite bridged by ionic liquid unit for glucose biosensing application. Sens Actuators, B: Chem 2012;161:728–33.
[42] Chen G, Takezawa M, Kawazoe N, Tateishi T. Preparation of cationic gold nanoparticles for gene delivery. Open Biotechnol J 2008;2:152–6.
[43] Kuila T, Mishra AK, Khanra P, Kim NH, Uddin MdE, Lee JH. Facile method for the preparation of water dispersible graphene using sulfonated poly(ether–ether–ketone) and its application as energy storage materials. Langmuir 2012;28:9825–33.
[44] Dreyer RD, Park S, Bielawski CW, Ruoff RS. The chemistry of graphene oxide. Chem Rev Soc 2010;39:228–40.
[45] Ferrari AC, Meyer JC, Scardaci V, Casiraghi C, Lazzeri M, Mauri F, et al. Raman spectrum of graphene and graphene layers. Phys Rev Lett 2006;97:187401.
[46] Zhang H, Feng PX. Fabrication and characterization of few-layer graphene. Carbon 2010;48:359–64.
[47] Meyer JC, Geim AK, Katsnelson MI, Novoselov KS, Booth JS, Roth S. The structure of suspended graphene sheets. Nature 2007;446:60–3.
[48] Jeong GH, Lee YW, Kim M, Han SW. High-yield synthesis of multi-branched gold nanoparticles and their surface-enhanced Raman scattering properties. J Colloid Interface Sci 2009;329:97–102.
[49] Shimizu T, Teranishi T, Hasegawa S, Miyake M. Size Evolution of alkanethiol-protected gold nanoparticles by heat treatment in the solid state. J Phys Chem B 2003;107:2719–24.
[50] Chen H, Kou X, Yang Z, Ni W, Wang J. Shape- and size-dependent refractive index sensitivity of gold nanoparticles. Langmuir 2008;24:5233–7.
[51] Chen ZJ, Ou XM, Tang FQ, Jiang L. Effect of nanometer particles on the adsorbability and enzymatic activity of glucose oxidase. Colloids Surf, B: Biointerfaces 1996;7:173–9.
[52] Yang H, Zhu Y. Size dependence of SiO_2 particles enhanced glucose biosensor. Talanta 2006;68:569–74.
[53] Wang G, Shen X, Wang B, Yao J, Park J. Synthesis and characterization of hydrophilic and organophilic graphene nanosheets. Carbon 2009;47:1359–64.
[54] Singh J, Srivastava M, Kalita P, Malhotra BD. A novel ternary $NiFe_2O_4$/CuO/FeO–chitosan nanocomposite as a cholesterol biosensor. Process Biochem 2012;47:2189–98.
[55] Hull RV, Li L, Xing YC, Chu CC. Pt nanoparticle binding on functionalized multiwalled carbon nanotubes. Chem Mater 2006;18:1780–8.
[56] Li J, Qiu JD, Xu JJ, Chen HY, Xia XH. The Synergistic effect of Prussian-blue-grafted carbon nanotube/poly(4-vinylpyridine) composites for amperometric sensing. Adv Funct Mater 2007;17:1574–80.
[57] Zhang H, Meng Z, Wang Q, Zheng J. A novel glucose biosensor based on direct electrochemistry of glucose oxidase incorporated in biomediated gold nanoparticles–carbon nanotubes composite film. Sens Actuators, B: Chem 2011;158:23–7.
[58] Shan CS, Yang HF, Song JF, Han DX, Ivaska A, Niu L. Direct electrochemistry of glucose oxidase and biosensing for glucose based on graphene. Anal Chem 2009;81:2378–82.
[59] Yadav SK, Singh J, Agrawal VV, Malhotra BD. Nanostructured nickel oxide film for application to fish freshness biosensor. Appl Phys Lett 2012;101:023703.
[60] Ricci F, Amine A, Palleschi G, Moscone D. Prussian blue based screen printed biosensors with improved characteristics of long-term lifetime and pH stability. Biosens Bioelectron 2003;18:165–74.
[61] Qu S, Wang J, Kong J, Yang P, Chen G. Magnetic loading of carbon nanotube/nano–Fe_3O_4 composite for electrochemical sensing. Talanta 2007;71:1096–102.
[62] Li L, Liang B, Li F, Shi J, Mascini M, Lang Q, Liu A. Co-immobilization of glucose oxidase and xylose dehydrogenase displayed whole cell on multiwalled carbon nanotube nanocomposite films modified electrode for simultaneous voltammetric detection of D-glucose and D-xylose. Biosens Bioelectron 2013;42:156–62.
[63] Dai ZH, Ni J, Huang XH, Lu GF, Bao JC. Direct electrochemistry of glucose oxidase immobilized on a hexagonal mesoporous silica-MCM-41 matrix. Bioelectrochemistry 2007;70:250–6.
[64] Zeng Q, Cheng J-S, Liu X-F, Bai H-T, Jiang J-H. Palladium nanoparticle/chitosan-grafted graphene nanocomposites for construction of a glucose biosensor. Biosens Bioelectron 2011;26:3456–63.
[65] Luo Z, Yuwen L, Han Y, Tian J, Zhu X, Weng L, Wang L. Reduced graphene oxide/PAMAM–silver nanoparticles nanocomposite modified electrode for direct electrochemistry of glucose oxidase and glucose sensing. Biosens Bioelectron 2012;36:179–85.
[66] Liu S, Tian J, Wang L, Luo Y, Lu W, Sun X. Self-assembled graphene platelet–glucose oxidase nanostructures for glucose biosensing. Biosens Bioelectron 2011;26:4491–6.
[67] Yang MH, Choi BG, Park HS, Hong WH, Lee SY, Park TJ. Development of a glucose biosensor using advanced electrode modified by nanohybrid composing chemically modified graphene and ionic liquid. Electroanalysis 2010;22:1223–8.
[68] Jang HD, Kim SK, Chang H, MinRoh K, Choi J-W, Huang J. A glucose biosensor based on TiO_2–graphene composite. Biosens Bioelectron 2012;38:184–8.
[69] Cheng N, Wang H, Li X, Yang X, Zhu L. Amperometric glucose biosensor based on integration of glucose oxidase with palladium nanoparticles/reduced graphene oxide nanocomposite. Am J Anal Chem 2012;3:312–9.